From Trioleoyl Glycerol to Extra Virgin Olive Oil through Multicomponent TriacylglycerolAG Mixtures: Crystallization and Polymorphic Transformation Examined with Differential Scanning Calorimetry and X-Ray RDiffration Techniques

L. Bayés-García,[a] T. Calvet,[a] M. A. Cuevas-Diarte[a] and S. Ueno[b]

[a]Secció de Cristal·lografia, Mineralogia i Dipòsits Minerals, Facultat de Ciències de la Terra, Universitat de Barcelona, Martí i Franquès s/n, E-08028 Barcelona, Spain

[b]Faculty of Applied Biological Science, Hiroshima University, Higashi-Hiroshima 739, Japan

Corresponding author: Laura Bayés-García (laurabayes@ub.edu)

25

26   **Abstract**

27

28   The polymorphic crystallization and transformation behavior of extra virgin olive oil

29   (EVOO) was examined by using differential scanning calorimetry (DSC) and X-ray

30   diffraction with both laboratory-scale (XRD) and synchrotron radiation source (SR-

31   XRD). The complex behavior observed was studied by previously analyzing mixtures

32   composed by its main 2 to 6 triacylglycerols (TAGs) components. Thus, component

33   TAGs were successively added to simulate EVOO composition, until reaching a 6 TAGs

34   mixture, composed by trioleoyl glycerol (OOO), 1-palmitoyl-2,3-dioleoyl glycerol

35   (POO), 1,2-dioleoyl-3-linoleoyl glycerol (OOL), 1-palmitoyl-2-oleoyl-3-linoleoyl

36   glycerol (POL), 1,2-dipalmitoyl-3-oleoyl glycerol (PPO) and 1-stearoyl-2,3-dioleoyl

37   glycerol (SOO). Molten samples were cooled from 25~~ºC~~ ºC to -80~~ºC~~ ºC at a controlled

38   rate of 2~~ºC~~ ºC/min and subsequently heated at the same rate. The polymorphic behavior

39   observed in multicomponent TAG mixtures was interpreted by considering three main

40   groups of TAGs with different molecular structures: triunsaturated OOO and OOL,

41   saturated-unsaturated-unsaturated POO, POL and SOO, and saturated-saturated-

42   unsaturated PPO. As confirmed by our previous work, TAGs belonging to the same

43   structural group displayed a highly similar polymorphic behavior. EVOO exhibited two

44   different β'-2L polymorphic forms (β'$_2$-2L and β'$_1$-2L), which transformed into β'-3L

45   when heated. Equivalent polymorphic pathways were detected when the same

46   experimental conditions were applied to the 6 TAG components mixture. Hence, minor

47   components may not exert a strong influence in this case.

48

49   **Keywords:** polymorphism; triacylglycerol; ~~lipid; mixture;~~ olive oil; differential scanning

2

50 calorimetry; X-ray diffraction; synchrotron radiation.

51

52 **1. Introduction**

53

54 Lipids are major nutrients and also widely used as lipophylic materials for diverse

55 applications, such as those related to food, cosmetic and pharmaceutical industries

56 (Larsson, Quinn, Sato, and Tiberg et al., 2006). Natural and industrial lipids are mostly

57 composed by a wide variety of triacylglycerols (TAGs), whose molecules involve

58 different fatty acid moieties (mixed-acid TAGs), giving rise to highly complex systems.

59 The physico-chemical properties of lipids, such as melting behavior, and textural and

60 rheological characteristics (Marangoni, and Narine et al., 2002), are mainly determined

61 by polymorphism, size, morphology and distribution of crystals arranged in fat crystal

62 networks. The complex polymorphic behavior exhibited by TAGs is strongly related to

63 the chemical nature of the fatty acid components: chain length, saturated/unsaturated

64 nature, cis/trans double bonds. Then, as most of natural and industrial lipids contain

65 different types of mixed-acid TAGs, their physicochemical properties must be

66 analyszed not only in single component systems, but also in mixed systems. For this

67 purpose, as an approach in order to understand the physical properties of complex real

68 fat systems, it is necessary to study the mixing behavior in binary (Boodhoo, Bouzidi,

69 and Narine et al., 2009; Bouzidi, Boodhoo, Kutek, Filip, and Narine et al., 2010; Ikeda,

70 Ueno, Miyamoto, and Sato et al., 2010; Mizobe et al., 2013; Bayés-García, Calvet,

71 Cuevas-Diarte, Ueno, and Sato et al., 2015), ternary (Sasaki, Ueno, and Sato et al.,

72 2012) and more complex mixture systems, which may be applied as basic knowledge to

73 delve into model fats and, at the end, final products.

3

74 An example of complex lipid system is olive oil. Among the different product

75 categories, extra virgin olive oil (EVOO) becomes a high-value agricultural product,

76 which is typical from the Mediterranean basin, and whose market has expanded to

77 North Europe, USA, China and Japan. The increasing popularity of this product has

78 mainly been attributed to its unique sensory, health and nutritional properties (Harwood,

79 and Yaqoob et al., 2002). EVOO is widely used as cooking oil and flavouring, but it is

80 also present in multiple formulated foods, such as sauces and dressings. Although

81 EVOO is liquid at room temperature, the crystallization characteristics of this low-

82 melting fat are important for the physical properties of foods employed at chilled

83 temperatures (e.g. frozen foods). Furthermore, understanding the crystallization and

84 polymorphic transformation behavior of EVOO, similarly to other lipid systems, may be

85 also applied for fractionation purposes (Timms, 2005; Salas, Bootello, Martínez-Force,

86 and Garcés et al., 2011) or even for the product authentication (Ferrari et al., 2007;

87 Bayés-García et al., 2016a) and the determination of food frauds (Chiavaro, Vittadini,

88 Rodriguez-Estrada, Cerretani, and Bendini, et al. 2008; Chiavaro et al., and 2009). At

89 this point, Chiavaro et al. the authors demonstrated the potential of differential scanning

90 calorimetry (DSC) as a technique to determine the presence of small amounts of

91 adulterant vegetable oils, such as refined hazelnut oil or high oleic sunflower oil, in

92 EVOO.

93 Previous work (Barba, Arrighetti, and Calligaris et al., 2013) examined the

94 crystallization and melting behavior of EVOO by using DSC and synchrotron radiation

95 X-ray diffraction (SR-XRD), in which very approximate conclusions were extracted

96 from the experimental data, as will be discussed further on. The authors proposed a

97 hexagonal crystal system for two β' forms observed $(\beta'_a$ and $\beta'_b)$ during EVOO

98 crystallization. However, these results were not consistent with those previously

4

99   reported, in which crystal systems of β' forms of pure TAGs were determined. As an

100   example, van Mechelen, Peschar, and Schenck et al. (2008) determined the β' crystal

101   structure of a series of mixed-acid TAGs containing palmitoyl, stearoyl and elaidoyl

102   acyl chains by using both laboratory-scale and synchrotron powder X-ray diffraction.

103   The results showed monoclinic cell setting in all cases. By contrast, spectroscopic

104   studies carried out on β' form of trisaturated 1,2-dipalmitoyl-3-myristoyl-*sn*-glycerol

105   (Yano et al., 1997) and triunsaturated trioleoyl glycerol (Akita, Kawaguchi, and Kaneko

106   et al., 2006), which becomes the main TAG in olive oil, showed that FT-IR bands

107   corresponded to orthorrombic orthorhombic perpendicular subcell, which is also against

108   the hexagonal symmetry supported by Barba, Arrighetti, and Calligaris (2013) et al.

109   Our group carried out a systematic study on the polymorphic behavior of the main

110   TAGs present in edible fats and oils, such as olive oil, having different molecular

111   structures: the unsaturated-saturated-unsaturated TAG 1,3-dioleoyl-2-palmitoyl glycerol

112   or OPO (Bayés-García, Calvet, Cuevas-Diarte, Ueno, and Sato et al., 2011); saturated-

113   unsaturated-saturated 1,3-dipalmitoyl-2-oleoyl glycerol or POP (Bayés-García, Calvet,

114   Cuevas-Diarte, Ueno, and Sato et al., 2013a); triunsaturated trioleoyl glycerol or OOO,

115   and 1,2-dioleoyl-3-*rac*-linoleoyl glycerol or OOL (Bayés-García, Calvet, Cuevas-

116   Diarte, Ueno, and Sato et al, 2013b); and saturated-unsaturated-unsaturated 1-

117   palmitoyl-2,3-dioleoyl glycerol or POO, 1-stearoyl-2,3-dioleoyl glycerol or SOO, and

118   1-palmitoyl-2-oleoyl-3-linoleoyl glycerol or POL (Bayés-García, Calvet, Cuevas-

119   Diarte, and Ueno et al., 2016b). In the present work, we characterized the polymorphic

120   behavior of EVOO with DSC and SR-XRD, by previously analyzing complex mixtures

121   composed by 2 to 6 TAG components. Studying multicomponent TAG mixtures of

122   main TAGs of olive oil permitted to understand in more detail the polymorphic

123   behavior of such a complex sample.

124

125 **2. Experimental**

126

127 Samples of trioleoyl glycerol (OOO), 1-palmitoyl-2,3-dioleoyl glycerol (POO), 1,2-

128 dioleoyl-3-linoleoyl glycerol (OOL), 1-palmitoyl-2-oleoyl-3-linoleoyl glycerol (POL),

129 1,2-dipalmitoyl-3-oleoyl glycerol (PPO) and 1-stearoyl-2,3-dioleoyl glycerol (SOO)

130 were purchased from Tsukishima Foods Industry (Tokyo, Japan) and used without

131 further purification (purity >99%). Extra virgin olive oil (EVOO), from the Arbequina

132 variety, was obtained from Coselva (cooperative from La Selva del Camp) and

133 harvested on December 2010.

134 To prepare the multicomponent TAG mixtures, TAG samples were melted at 50ºC ºC

135 and mixed using a vortex. Jiménez Márquez, and Beltrán Maza et al. (2003), and

136 Jiménez Márquez, Beltrán Maza, Aguilera Herrera, and Uceda Ojeda (2007) determined

137 the TAGs composition of olive oils obtained from different olive varieties. Following

138 the data presented by the authors, mixtures containing from 2 to 6 main TAGs present

139 in olive oil of the Arbequina variety were prepared. In order to determine the percentage

140 (wt/wt) of each TAG, mean values of the concentration ratios extracted from the

141 literature were calculated and extrapolated to 100%. Table 1 shows the concentration

142 values (% wt/wt) used to prepare the TAG mixtures, together with compositional data

143 from previous works.

144

145 **Table 1.** Concentration ratios (% wt/wt) of TAGs present in multicomponent TAG mixtures. Previously

146 reported data are is also shown.

Multicomponent TAG mixtures		Arbequina virgin olive oil

6

	2 TAGs	3 TAGs	4 TAGs	5 TAGs	6 TAGs	Jiménez et al. (2003)	Jiménez et al. (2007)
OOO	58	47	41	39	38	38.1	32.4
POO	42	31	27	26	25	22.9	24.6
OOL		22	20	19	19	17.6	16.8
POL			12	11	11	9.3	10.6
PPO				5	4	3.2	5.1
SOO					3	3.1	2.7

147

148 TAG compositions of the samples were determined by High Performance Liquid

149 Chromatography (HPLC). The chromatograph used was an Agilent-1100 with

150 thermostatic control of column temperature and equipped with a differential

151 refractometry detector. A Kinetex column (250 mm long x 4.6 mm i.d.) with C18

152 reverse phase (particle size 5mm) (Phenomenex) was used. TAGs were eluted using a

153 gradient according to the following procedure: mobile phase A acetonitrile and B

154 acetone (50:50), with isocratic gradient during the full analysis. The flow rate was 1

155 ml/min. TAGs were identified by their equivalent carbon number (ECN) calculated as

156 follows: $ECN = CN - 2NDB$, where CN is the carbon number and NDB is the number

157 of double bonds of the TAG. Data were analyzed with HPLC ChemStation software.

158 DSC experiments were conducted at atmospheric pressure using a Perkin-Elmer

159 DSC-7. Samples (9.0-9.4 mg) were weighed into 50 µl aluminum pans and covers

160 were sealed into place. The instrument was calibrated with reference to the enthalpy

161 and the melting points of indium (melting temperature, 156.6ºC; ΔH, 28.45 J/g)

162 and decane (melting temperature, -29.7ºC; ΔH, 202.1 J/g) standards. An empty

163 pan was used as reference. Dry nitrogen was used as purge gas in the DSC cell at 23

164 cm^3/min. Thermograms were analyzed with Pyris software to obtain the enthalpy

7

165 (J/g, integration of the DSC signals) and T_{onset} of the transitions (°C, intersections

166 of the baseline and the initial tangent at the transition). The molten samples were

167 cooled from 25 °C to -80 °C at 2 °C/min and subsequently heated from -80

168 °C to 25 °C at the same rate. At least three independent measurements were made

169 for each experiment (n = 3). Random uncertainty was estimated with a 95%

170 threshold of reliability using the Student's t-distribution, which enables estimation

171 of the mean of a normally distributed population when it is small.

172 SR-XRD experiments with simultaneous measurements of small- and wide-angle X-ray

173 diffraction (SAXD and WAXD) were carried out at the BL-6A of the synchrotron

174 radiation facility Photon Factory (PF) at the High-Energy Accelerator Research

175 Organization (KEK) in Tsukuba (Japan). A double-focusing camera operated at a

176 wavelength of 0.15 nm and the X-ray scattering data were simultaneously collected by

177 two-dimensional semiconductor PILATUS-2M (Dektoris Co., Switzerland) for SAXD

178 and PILATUS-100K for WAXD. Camera lengths were 900 mm for SAXD and 270 mm

179 for WAXD. Each temperature program was controlled by a Linkam THMSF-600 stage

180 (LINKAM Co., Cambridge, U.K.) and a 1-mm-thick sample was placed in an aluminum

181 sample cell with Kapton film windows. Tripalmitin (PPP) and trilaurin (LaLaLa) were

182 used as calibrants and data were processed with in-house software provided by the

183 Laboratory of Food Biophysics of the Hiroshima University. SR-XRD spectra were

184 acquired at 60s intervals.

185 Laboratory-scale powder XRD experiments were performed by using a PANalytical

186 X'Pert Pro MPD powder diffractometer equipped with an

187 X'Celerator Detector. The equipment also included an Oxford Cryostream Plus 220V

188 (temperature 80 to 500K). Monochromatic Cu Kα_1 (λ = 0.154059 nm) radiation was

189 selected by means of a Hybrid Monochromator. This diffractometer operated with

190 Debye-Scherrer transmission geometry and. tThe sample was introduced in a 1mm-

191 diameter Lindemann glass capillary. The latter was rotated about its axis during the

192 experiment to minimize preferential orientations of the crystallites. The step size was

193 0.013º from 1.004º to 28º 2θ and the measuring time was 150 seconds per pattern.

194 X'Pert HighScore software was used to process XRD data.

195

196 **3. Results and Discussion**

197

198 Figure 1 qualitatively shows compositional modifications of multicomponent mixtures

199 when component TAGs were progressively added.
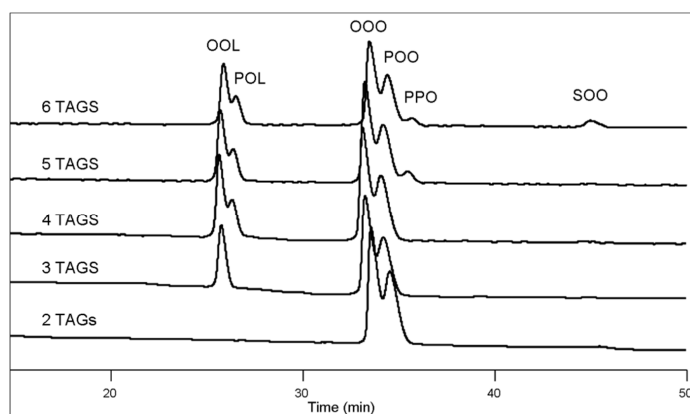
200

201

202

203 **Figure 1.** HPLC chromatograms of multicomponent TAG mixtures containing from 2 to 6 TAGs.

204

205

206 Although very slight differences were detected in some cases, HPLC results confirmed

207 the TAG concentrations of the previously prepared mixtures, although slight differences

9

208 ~~were detected in some cases, which were within the experimental error~~. Table 2

209 summarizes the TAG composition of the prepared mixtures, determined by HPLC.

210

211 **Table 2.** TAG composition (% wt/wt) of multicomponent mixtures determined by HPLC.

	2 TAGs	3 TAGs	4 TAGs	5 TAGs	6 TAGs
OOO	54	44	37	36	35
POO	46	33	29	28	26
OOL		23	21	21	21
POL			12	10	10
PPO				5	4
SOO					4

212

213 The DSC thermograms obtained when samples containing from 1 to 6 TAG

214 components and EVOO sample were cooled from 25~~ºC~~ ºC to -80~~ºC~~ ºC at 2~~ºC~~ ºC/min

215 and subsequently heated at the same conditions are shown in Figure 2. Table 3

216 summarizes onset temperatures (T_{onset}) and enthalpy (ΔH) values associated to each

217 thermal phenomenon. Figure 3 depicts the temperature-dependent laboratory-scale XRD

218 patterns, corresponding to mixtures containing from 2 to 5 TAG components.
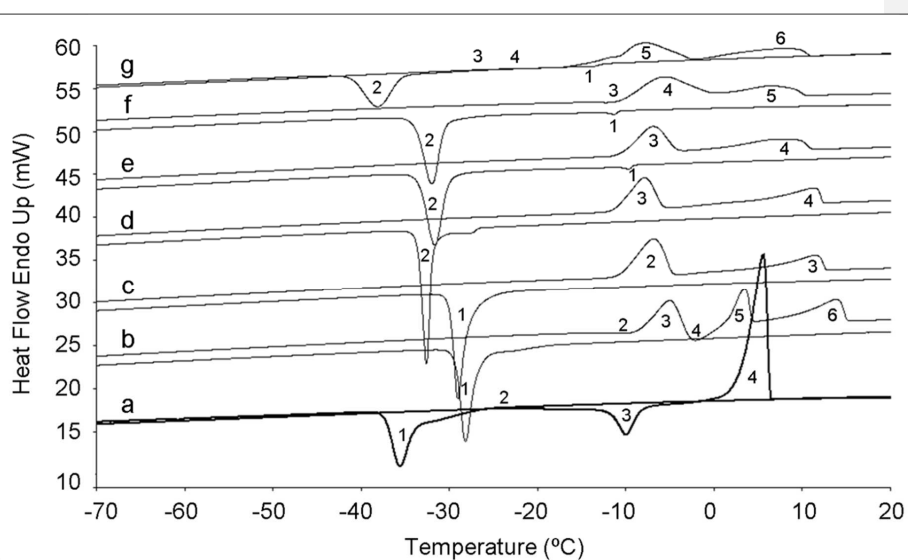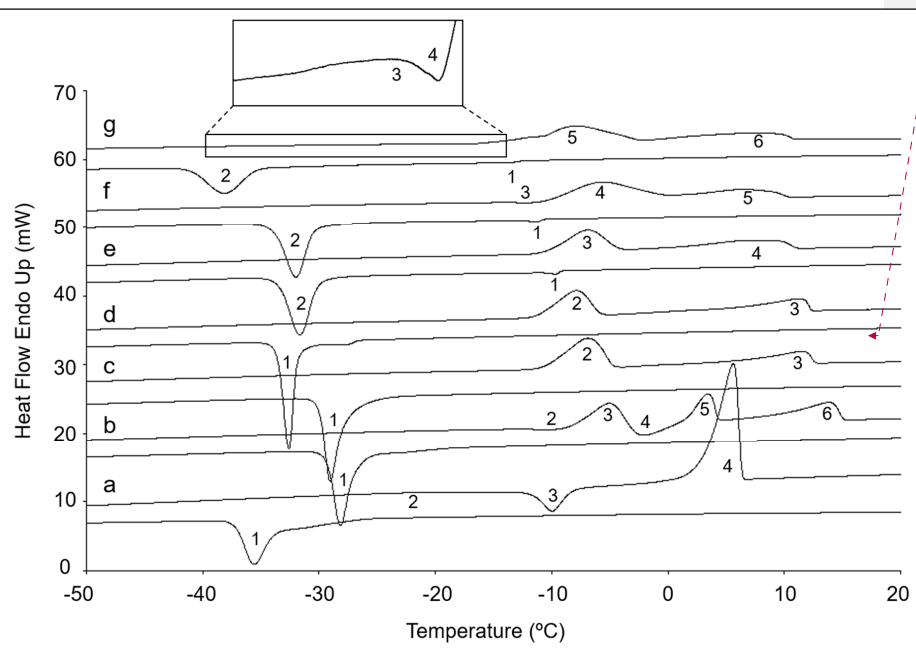
219

10

Figure 2. DSC (cooling and heating curves) plot of multicomponent TAG mixtures and EVOO

(Arbequina variety). a) 1 TAG (100% OOO). b) 2 TAGs (58% OOO + 42% POO). c) 3 TAGs (47%

OOO + 31% POO + 22% OOL). d) 4 TAGs (41% OOO + 27% POO + 20% OOL + 12% POL). e) 5

225 TAGs (39% OOO + 26% POO + 19% OOL + 11% POL + 5% PPO). f) 6 TAGs (38% OOO + 25% POO

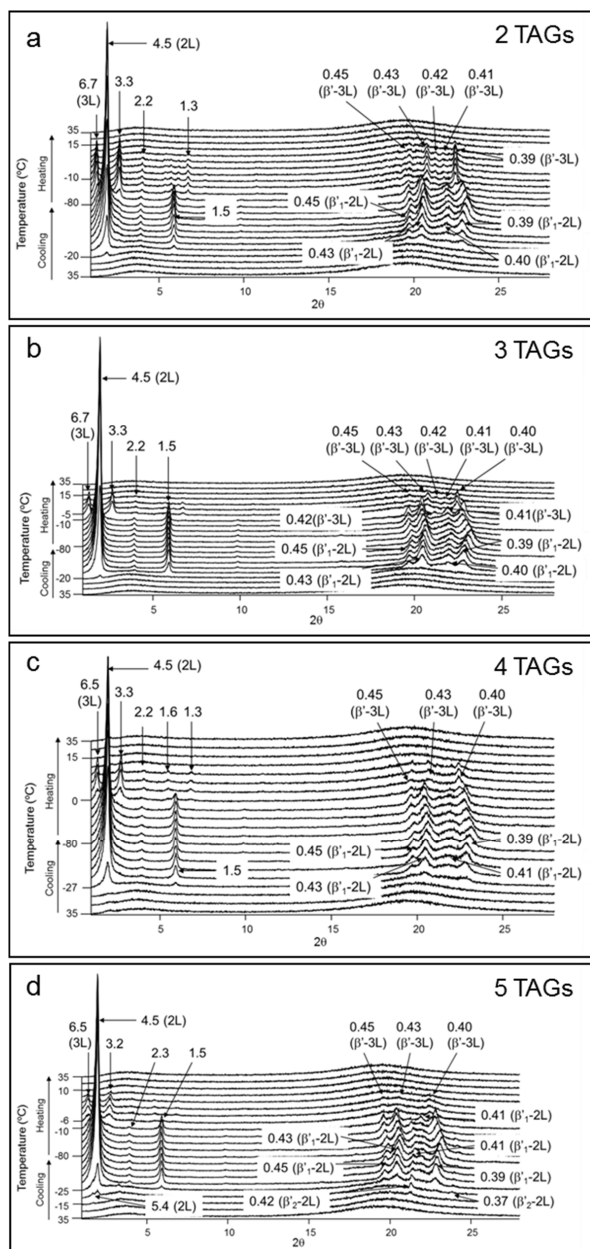226 + 19% OOL + 11% POL + 4% PPO + 3% SOO). g) EVOO.

227

228

229

230 **Table 3.** DSC data corresponding to the crystallization, polymorphic transformation and melting

231 processes of OOO (1 TAG), TAG mixtures from 2 to 6 TAGs and EVOO (Arbequina variety) obtained

232 when samples were cooled and heated at 2ºC ºC/min. Letters *c* and *m* mean *crystallization* and *melting*,

233 respectively. DSC peaks were labelled according to their exothermic (*exo*) or endothermic (*endo*) nature.

		Cooling (~~2ºC~~ ºC/min)		Heating (~~2ºC~~ ºC/min)				
1 TAG		*1 (β'_2 (c))*		*2 ($\beta'_2 \to \beta_2$)*	*3 ($\beta_2 \to \beta_1$)*	*4 ($\beta_2 + \beta_1$ (m))*		
	T_{onset} (ºC)	-26.6 ± 1.2	-33.4 ± 0.7	-25.0 ± 1.7	-11.3 ± 1.7	-2.2 ± 0.7	2.9 ± 1.3	
	ΔH (J/g)	-70 ± 1		n.d.	-27 ± 4	128 ± 5**		
2 TAGs		*1 (exo)*		*2 (exo)*	*3 (endo)*	*4 (exo)*	*5 (endo)*	*6 (endo)*
	T_{onset} (ºC)	-18.6 ± 1.7	-26.8 ± 0.2	-13.3 ± 0.5	-8.1 ± 0.7	-3.3 ± 0.7	1.4 ± 0.5	6.3 ± 1.0
	ΔH (J/g)	-76 ± 3		-3 ± 1	31 ± 3	-11 ± 7	69 ± 9**	
3 TAGs		*1 (exo)*		*2 (endo)*	*3 (endo)*			
	T_{onset} (ºC)	-25.1 ± 1.4		-10.6 ± 0.4	-4.7 ± 1	3.4 ± 0.8		
	ΔH (J/g)	-76 ± 3		90 ± 3**				
4 TAGs		*1 (exo)*		*~~3~~ 2 (endo)*	*~~4~~ 3 (endo)*			
	T_{onset} (ºC)	-26.6 ± 0.4	-31.9 ± 0.3	-11.4 ± 0.5	-6.6 ± 1.6	1.6 ± 0.8		
	ΔH (J/g)	-70 ± 2		88 ± 4**				
		1 (exo)	*2 (exo)*	*3 (endo)*	*4 (endo)*			

12

		1 (exo)	2 (exo)	3	4	5	6
5 **TAGs**	T_onset (°C)	-9.0 ± 0.4	-30.0 ± 0.3	-10.3 ± 0.5	-2.8 ± 0.5		
	ΔH (J/g)	-70 ± 3**		85 ± 2**			
		1 (exo)	*2 (exo)*	*3 (exo)*	*4 (endo)*	*5 (endo)*	
6 **TAGs**	T_onset (°C)	-10.6 ± 0.5	-30.5 ± 0.3	-14.0 ± 0.6	-10.2 ± 0.5	-1.6 ± 0.5	
	ΔH (J/g)	-70 ± 3**		-1 ± 1	85 ± 3**		
		1 (exo)	*2 (exo)*	*3 (endo)*	*4 (exo)*	*5 (endo)*	*6 (endo)*
EVOO **Sample**	T_onset (°C)	-12.4 ± 0.4	-35.4 ± 0.3	-28.5 ± 0.8*	-25.2 ± 1.3	-17.2± 0.3 - 11.5±0.7	-3.7 ± 0.6
	ΔH (J/g)	-65 ± 8**		---	-4 ± 1	77 ± 4**	

n.d. Not determined

Two T_onset values were assigned to some DSC peaks due to the presence of shoulders, although some of them could not be clearly appreciated through Figure 2. *The peak top temperature was determined in this case. No ΔH value was given for this peak, as the onset and end temperatures could not be clearly defined. ** These enthalpy values correspond to the global enthalpy of the overlapped peaks.

239

Figure 3. Laboratory-scale XRD patterns of multicomponent TAG mixtures from 2 to 5 TAG

components. a) 2 TAGs (58% OOO + 42% POO). b) 3 TAGs (47% OOO + 31% POO + 22% OOL). c) 4

242 TAGs (41% OOO + 27% POO + 20% OOL + 12% POL). d) 5 TAGs (39% OOO + 26% POO + 19%

243 OOL + 11% POL + 5% PPO).

244

245 Previous work reported by our group analyzed the influence of dynamic thermal

246 treatments on the complex polymorphic behavior of OOO (Bayés-García, Calvet,

247 Cuevas-Diarte, Ueno, and Sato ~~et al.~~, 2013b). The SR-XRD data revealed that, when

248 OOO was cooled from the melt at 2~~ºC~~ °C/min, the crystallizing polymorph was β'_2.

249 However, the DSC cooling curve showed a complex phenomenon consisting of a main

250 exothermic peak with T_{onset} at -33.4~~ºC~~ °C having a shoulder at -26.6~~ºC~~ °C (peak 1 in

251 Figure 2a), which revealed the beginning of the crystallization process (see Table 3).

252 When β'_2 crystals were subsequently heated at 2~~ºC~~ °C/min, two consecutive transitions

253 occurred: β'_2 form transformed into β_2 form at around -25.0~~ºC~~ °C (peak 2 in Figure 2a)

254 and, on further heating, a solid-state transformation from β_2 to most stable β_1 form was

255 detected at -11.3~~ºC~~ °C (peak 3 in Figure 2a). Finally, two slightly separated melting

256 phenomena were observed, corresponding to the melting of some remaining β_2 form

257 (T_{onset}=-2.2~~ºC~~ °C) and β_1 form (T_{onset}=2.9~~ºC~~ °C).

258 By adding more TAG components to OOO, the complexity of the polymorphic behavior

259 increased considerably. Thus, when POO was added to OOO (2 TAGs mixture

260 composed by 58% OOO and 42% POO) and the mixture was cooled at 2~~ºC~~ °C·min^{-1}, a

261 broad exothermic peak with two onset temperatures, at -18.6~~ºC~~ °C and -26.8~~ºC~~ °C,

262 appeared in the DSC cooling curve (peak 1 in Figure 2b and Table 3). Therefore, the

263 addition of POO caused a shifting of the crystallization peak to higher temperatures.

264 The corresponding XRD pattern (Figure 3a) revealed the occurrence of a β' form (short

265 spacing values of 0.45 nm, 0.43 nm, 0.40 nm and 0.39 nm), having a double chain

266 length structure (long spacing value of 4.5 nm). This β' form, having a double chain

15

267 length structure, was tentatively called β'$_1$-2L form, as an additional β'-2L form

268 occurred when TAGs were successively added, as will be discussed further on. No new

269 XRD peaks were observed during the cooling process. Thus, we may think that OOO

270 and POO did not crystallized separately, so that an alloy between the two component

271 TAGs may have been formed. Complicated transformation processes were observed in

272 the DSC curve corresponding to the subsequent heating step. A small exothermic DSC

273 peak, with an enthalpy value of -3 J/g, was observed at a T$_{onset}$ of -13.3 °C. This peak

274 was followed by an endothermic peak at -8.1 °C (peak 3 in Figure 2b), an exothermic

275 phenomenon with T$_{onset}$ at -3.3 °C (peak 4), and two consecutive endothermic peaks

276 at 1.4 °C and 6.3 °C (peaks 5 and 6, respectively). The XRD data only showed, at

277 approximately -10 °C, the occurrence of a triple chain length structure peak at 6.7 nm,

278 corresponding to a β'-3L form (new wide angle region peaks appeared at 0.45 nm, 0.43

279 nm, 0.42 nm, 0.41 nm and 0.39 nm). On further heating, the double chain length peak at

280 4.5 nm totally vanished at 2 °C (corresponding to the β'$_1$-2L form melting), and the

281 β'-3L peaks disappeared at around 15 °C (β'-3L melting). One may consider that the

282 long spacing value of the last melting form could correspond to a β'$_{POO}$ form (Bayés-

283 García, Calvet, Cuevas-Diarte, and Ueno, 2016b). As to OOO, chain length

284 structures of all polymorphic forms of OOO are double, having a long spacing value of

285 4.5 or 4.4 nm (Bayés-García, Calvet, Cuevas-Diarte, Ueno, and Sato, 2013b), so

286 judging from the short spacing values, some β'$_{OOO}$ should be present. However, only

287 one crystallizing polymorph was obtained from the melt by cooling the 2 TAGs mixture

288 at 2 °C/min. A possible explanation of the phenomena observed is the crystallization

289 of a metastable alloy of the two component TAGs. When heating, this alloy probably

290 melted and individual TAGs crystallized (melt-mediated transformation). Finally, β'$_{OOO}$

16

291 melted at around 1.4ºC °C (peak 5), followed by the melting of β'$_{POO}$ at 6.3ºC °C (peak

292 6) (T$_{onset}$ values).

293 By adding OOL, the DSC heating curve became simpler than that of the 2 TAGs

294 mixture, and more similar to that of EVOO. As to the laboratory-scale XRD patterns,

295 they became almost identical to that of the 2 TAGs mixture. Thus, by cooling the 3

296 TAGs mixture at 2ºC °C·min^{-1}, a clear exothermic peak, with a single onset temperature

297 at -25.1ºC °C, appeared in the DSC cooling curve (peak 1 in Figure 2c). Simultaneously,

298 laboratory-scale XRD data showed the occurrence of the β'$_1$-2L form previously

299 described, which was identified by a double chain length peak at 4.5 nm and wide short

300 angle diffraction peaks at 0.45 nm, 0.43 nm, 0.40 nm and 0.39 nm. When the sample

301 was heated, an endothermic peak appeared at around -10.6ºC °C (peak 2) and it was

302 followed by a broader one (peak 3) characterized by two onset temperatures at -4.7ºC °C

303 and 3.4ºC °C, respectively. XRD data revealed, at approximately -5ºC °C, the

304 occurrence of a new β'-3L form at the expense of β'$_1$-2L form. The newly formed β'-3L

305 phase was detected by the presence of a triple chain length peak at 6.7 nm and wide

306 short angle diffraction peaks at 0.45 nm, 0.43 nm, 0.41 nm at 0.40 nm. XRD peaks of

307 this β'-3L form totally vanished at 15ºC °C. Similarly to the 2 TAGs mixture case, when

308 the sample was cooled, probably some molecular alloy of the three TAG components

309 (OOO, POO and OOL) was formed. However, it transformed to a more stable β'-3L

310 form when heated. By considering the phenomena observed in the DSC heating

311 thermogram and the slight increase of background in the corresponding XRD diffraction

312 patterns, one may conclude that this β'$_1$-2L→β'-3L polymorphic transformation most

313 probably may have occurred through the liquid state (melt-mediated transformation).

314 No important changes were observed when POL was added. Figures 2d and 3c depict

315 the DSC thermogram of the 4 TAGs mixture and the corresponding XRD patterns,

316 respectively. When the 4 TAGs mixture was cooled at 2~~ºC~~ ºC/min, again β'$_1$-2L form

317 was detected by the corresponding XRD peaks at 4.5 nm, and 0.45 nm, 0.43 nm, 0.41

318 nm and 0.39 nm in the ~~short~~ small and wide angle regions, respectively. The

319 corresponding exothermic DSC peak became different from that of the 3 TAGs mixture,

320 as it consisted of a double crystallization peak with two clear onset temperatures at -

321 26.6~~ºC~~ ºC and -31.9~~ºC~~ ºC. Furthermore, the addition of POL caused a shifting of the

322 main crystallization peak to lower temperatures (see Figure 2). As to the heating

323 process, again only two endothermic peaks appeared in the DSC curve. The first one

324 was detected at a T$_{onset}$ of -11.4~~ºC~~ ºC, and two different onset temperatures (-6.6~~ºC~~ ºC

325 and 1.6~~ºC~~ ºC) were determined for the second endothermic peak (peak 3 in Figure 3d).

326 Similarly to all the previous mixtures discussed, the XRD data revealed the occurrence

327 of a β'-3L form at the expense of β'$_1$-2L form, at around 0~~ºC~~ ºC. In this case, the long

328 spacing value of the triple chain length structure was 6.5, instead of 6.7, and β' peaks at

329 0.45 nm, 0.43 nm and 0.40 nm were also present. Finally, the β'-3L XRD peaks

330 vanished at 10~~ºC~~ ºC.

331 By comparing the DSC thermograms of multicomponent TAG mixtures containing

332 from 2 to 4 TAGs, one may notice progressive changes as TAGs were successively

333 added. Most important variations were observed when OOL was included in the system,

334 as three endothermic peaks appeared in the DSC heating curve of the 2 TAGs mixture,

335 whereas only two were observed in the 3 TAGs mixture case. As already noted, the

336 metastable alloy formed when the 2 TAGs mixture was cooled may have transformed

337 into individual β' forms of TAG components during the subsequent heating process.

338 However, this behavior was not observed when OOL was added, as the initially formed

339 β'$_1$-2L polymorph may have transformed into a single β'-3L when heated, which finally

340 melted on further heating. The same polymorphic behavior was observed when the 4

341 TAGs mixture was anal~~yz~~sed. At this point, one may take into account the structural

342 similarity between some of the TAG components. A similar polymorphic behavior was

343 observed, on the one hand, in triunsaturated TAGs (such as OOO and OOL) (Bayés-

344 García, Calvet, Cuevas-Diarte, Ueno, and Sato ~~et al.~~, 2013b) and, on the other hand, in

345 saturated-unsaturated-unsaturated TAGs (like POO and POL) (Bayés-García, Calvet,

346 Cuevas-Diarte, and Ueno ~~et al.~~, 2016b). Thus, in general, with the addition of new

347 TAGs to the mixtures, no considerable changes were appreciated, especially in the XRD

348 patterns. Only β'$_1$-2L and β'-3L forms were detected in the laboratory scale XRD data,

349 due to different polymorphic behavior caused by two groups of TAGs: triunsaturated

350 OOO and OOL and saturated-unsaturated-unsaturated POO and POL.

351 More appreciable changes were noted when a saturated-saturated-unsaturated (PPO)

352 TAG was added. Figures 2e and 3d show the DSC thermogram and the corresponding

353 XRD patterns of the 5 TAGs mixture (composed by OOO, POO, OOL, POL and PPO),

354 respectively. Two crystallization processes were observed in the DSC cooling curve.

355 The first one occurred at -9.0~~ºC~~ ºC, which corresponded to higher temperatures than

356 those of mixtures up to 4 TAG components, as described above. Simultaneously, the

357 XRD ~~wide~~ small angle region exhibited a double chain length peak at 5.3 nm, whereas

358 β' form peaks appeared in the wide angle region, at 0.42 nm and 0.37 nm. This β' form,

359 named β'$_2$-2L form, may be caused by the presence of PPO. On further cooling, at -

360 30.0~~ºC~~ ºC, β'$_1$-2L crystallization was observed, as XRD data revealed by the occurrence

361 of a double chain length peak at 4.5 nm and ~~short~~ wide angle peaks at 0.45 nm, 0.43 nm,

362 0.41 nm and 0.39 nm. When heating, at -10~~ºC~~ ºC, β'$_2$-2L form peaks vanished, due to

363 its melting or some polymorphic transformation. Right after, at -6~~ºC~~ ºC, new β'-3L

364 XRD peaks appeared, at the expense of β'$_1$-2L peaks, at 6.5nm in the ~~wide~~ small -angle

365 region, and at 0.45 nm, 0.43 nm and 0.40 nm in the ~~short~~ wide angle region. No XRD

19

366 peaks were present at 10ºC °C, revealing the melting of β'-3L form. As to the DSC data,

367 only two broad endothermic peaks with T_{onset} at -10.3ºC °C (peak 2 in Figure 2e) and -

368 2.8ºC °C (peak 3), respectively, appeared in the DSC heating curve. Thus, complex

369 phenomena took place within the same temperature ranges, obtaining broad responses

370 by the DSC. One may pay attention to the flatness of the DSC signals if they are

371 compared to those of the 4 TAGs mixture.

372 As to the 6 TAGs mixture, no considerable differences were observed when SOO was

373 added. We should remind the saturated-unsaturated-unsaturated structure of this TAG,

374 which may display a similar polymorphic behavior to that of POO and POL. Figure 2f

375 depicts the corresponding DSC thermogram, whereas time-dependent XRD patterns are

376 shown in Figure 4a. For this sample, SR-XRD with SAXD and WAXD measurements

377 were carried out (Figures 4b and 4c), and the results obtained could be compared with
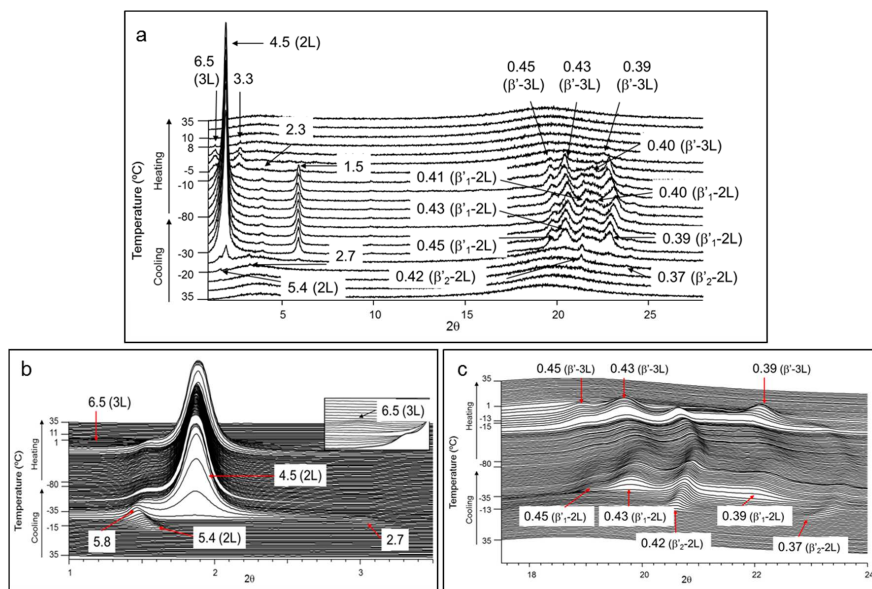
378 those of laboratory-scale XRD data.

379

380

381

382   **Figure 4.** XRD patterns of multicomponent TAG mixture of 6 TAG components (38% OOO + 25% POO

383   + 19% OOL + 11% POL + 4% PPO + 3% SOO). a) Laboratory-scale XRD. b) SR-SAXD pattern. c) SR-

384   WAXD pattern.

385

386   Similarly to the mixture containing 5 TAG components, by cooling the 6 TAGs mixture

387   at 2 °C/min, a β'$_2$-2L crystallization occurred at -10.6 °C. Both laboratory-scale

388   XRD and SR-XRD data revealed a double chain length structure peak at 5.4 nm, and the

389   small angle region showed typical β' form peaks at 0.42 and 0.37 nm. On further

390   cooling, another exothermic peak at -30.5 °C was detected in the DSC cooling curve

391   (see Figure 2f), corresponding to an additional β'$_1$-2L form crystallization, with long

392   and short spacing values of 4.5nm, and 0.45 nm, 0.43 nm and 0.39 nm, respectively

393   (Figure 4). As to the heating step, and differently from the previous TAGs mixtures

394   examined, an exothermic DSC peak (peak 2 in Figure 2f), having an onset temperature

395   of -14.0 °C, preceded the first broad endothermic peak at -10.2 °C. Within this

396   temperature range, at -13 °C, the SR-XRD data clearly revealed the extinction of β'$_2$-

397   2L peaks at 0.42 nm and 0.37 nm. At approximately -5 °C, triple chain length

398   structure peak at 6.5 nm, corresponding to a β'-3L form, appeared at the expense of the

399   double chain length structure peak at 4.5 nm. The broad endothermic DSC signal,

400   labelled as peak 5 in Figure 2f, had a T$_{onset}$ of -1.6 °C. XRD data revealed the total

401   extinction of β'$_1$-2L peaks at around 1 °C, whereas β'-3L peaks disappeared at

402   approximately 11 °C.

403   Finally, EVOO sample was examined by following the same procedure (Figure 5). No

404   significant differences were detected in the corresponding DSC cooling and heating

405   curves (Figure 2g) compared to the thermal response of the 6 TAGs mixture sample

406   (Figure 2f), and the respective XRD patterns were almost identical (compare Figures 4

407 and 5). This fact revealed a weak influence of the minor compounds present in the olive
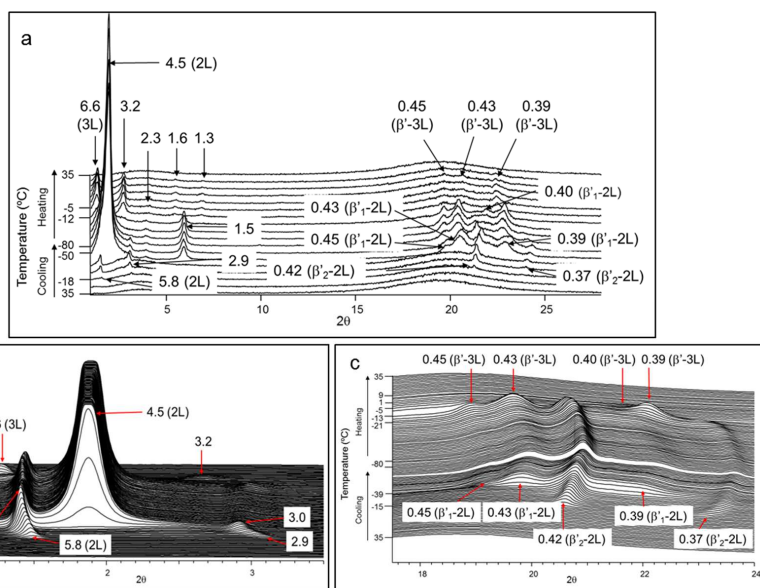
408 oil sample.

409

412 **Figure 5.** XRD patterns of EVOO (Arbequina variety). a) Laboratory-scale XRD. b) SR-SAXD pattern.

413 c) SR-WAXD pattern.

414

415 By cooling the EVOO sample at a rate of 2ºC ºC/min, β'_2-2L form crystallized from the

416 melt at -12.4ºC ºC (peak 1 in Figure 2g). Short spacing values of this β'_2-2L form were

417 the same as those of the 6 TAGs mixture (0.42 nm and 0.37 nm), whereas the long

418 spacing value became higher (5.8 nm), as confirmed by both laboratory-scale XRD and

419 SR-XRD. On further cooling, the main crystallization peak, corresponding to the

420 crystallization of β'_1-2L form (4.5nm, and 0.45 nm, 0.43 and 0.39 nm) appeared at

421 lower temperatures (T_{onset}= -35.4ºC ºC) compared to that of the mixture of 6 TAG

422 components. When the crystallized olive oil was subsequently heated at 2ºC ºC/min, a

22

423 broad endothermic peak, with peak top temperature of -28.3°C °C, followed by an

424 exothermic peak with T_{onset} of -25.2°C °C were observed. The DSC heating thermogram

425 also exhibited an endothermic peak with a shoulder, which defined two onset

426 temperatures of -15.5°C °C and -11.3°C °C. Within this temperature range, at -13°C °C,

427 XRD peaks at 5.8 nm, 2.9 nm, and 0.42 nm, 0.37 nm, corresponding to β'$_2$-2L form,

428 vanished. Later, at -5°C °C, triple chain length structure peak at 6.6 nm (β'-3L)

429 appeared after the intensity of the double chain length structure peak at 4.5 nm

430 decreased. Simultaneously, the SR-XRD data clearly showed, through the WAXD

431 pattern, the occurrence of β' peak at 0.40 nm. On further heating, a broad DSC signal

432 with T_{onset} of -3.7°C °C (peak 5 in Figure 2g) was observed. In addition, XRD results

433 revealed the total disappearance of β'$_1$-2L and β'-3L forms at around 1°C °C and 11°C

434 °C, respectively.

435 Barba, Arrighetti, and Calligaris et al. (2013) reported on the crystallization and melting

436 behavior of extra virgin olive oil by using DSC and SR-XRD. In the mentioned work,

437 only very approximate conclusions were extracted from the experimental data. The

438 results showed in the present study are in discordance with those discussed by Barba,

439 Arrighetti, and Calligaris (2013) et al., due to different interpretation of the SR-XRD

440 data. The authors described the crystallization of two β' forms when an extra virgin

441 olive oil sample was cooled at 2°C °C/min, which partly transformed into most stable β

442 form when heating. This polymorphic transformation was identified through the WAXD

443 pattern, as no new SAXD peaks were detected. In the present work, no β form was

444 detected during the heating step, as the hypothetic most stable β form described by

445 Barba Arrighetti, and Calligaris (2013) et al. was interpreted as β'-3L form in the present

446 work. However, one may also consider that the different polymorphic behavior

447 observed could also be due to a different TAG composition of the two EVOO samples.

23

448 The study of multicomponent TAG mixtures by using the main TAGs of olive oil

449 permitted to understand in more detail the polymorphic behavior of such a complex

450 sample.

451 Figure 6 depicts a summary of the polymorphic crystallization and transformation

452 pathways exhibited by 1 TAG to 6 TAGs mixture and EVOO samples when they were

453 cooled and subsequently heated at 2ºC ºC/min.

454

	COOLING	HEATING
1 TAG	liquid $\longrightarrow$ β'_2-2L (OOO)	β_2-2L (OOO) $\longrightarrow$ β_1-2L (OOO) $\longrightarrow$ liquid
2 TAGs	liquid $\longrightarrow$ β'_1-2L $\longrightarrow$ liquid	$\longrightarrow$ β'-2L (OOO) / $\longrightarrow$ β'-3L (POO) $\longrightarrow$ liquid
3 TAGs 4 TAGs	liquid $\longrightarrow$ β'_1-2L $\longrightarrow$ liquid	$\longrightarrow$ β'-3L $\longrightarrow$ liquid
5 TAGs 6 TAGs EVOO	liquid $\longrightarrow$ β'_2-2L + β'_1-2L	$\longrightarrow$ liquid $\longrightarrow$ β'-3L $\longrightarrow$ liquid

455

456 **Figure 6.** Polymorphic crystallization and transformation pathways of 1 TAG to 6 TAGs mixture and

457 EVOO samples.

458

459 The DSC results plotted in Figure 2 graphically showed the influence of every TAG

460 component. Most important differences were observed when OOL was added to the 2

461 TAGs mixture (composed by OOO and POO), as the complex DSC heating curve

462 including exothermic and endothermic peaks (see Table 3) changed to a DSC profile

463 based on two broad endothermic peaks. The different thermal behavior observed may be

24

464 explained by considering the different polymorphic pathways shown in Figure 6. When

465 the molten 2 TAGs mixture was cooled at 2~~ºC~~ ºC/min, a β'$_1$-2L metastable alloy formed

466 by OOO and POO crystallized, which melted when heated, and individual TAGs

467 crystallized (melt-mediated transformation) in β'-2L (OOO) and β'-3L (POO) forms.

468 The same crystallization behavior was observed when the molten 3 TAGs mixture was

469 cooled. However, a single melt-mediated polymorphic transformation occurred from

470 β'$_1$-2L to β'-3L. The same polymorphic behavior was observed when the 4 TAGs

471 mixture was subjected to the same experimental conditions.

472 More variations were detected when PPO (a saturated-unsaturated-unsaturated TAG)

473 was added to the 4 TAGs mixture (OOO, POO, OOL and POL). At this point, a new

474 exothermic DSC peak appeared at around -30~~ºC~~ ºC, which was due to the crystallization

475 of an additional β'$_2$-2L form, as laboratory-scale XRD and SR-XRD data confirmed.

476 The increasing complexity of the multicomponent TAG mixtures was reflected in the

477 DSC thermograms, as broader and flatter signals appeared while increasing the number

478 of TAGs. The same polymorphic pathways were observed in samples of 6 TAGs

479 mixture and EVOO.

480 The complex polymorphic behavior observed in multicomponent TAG mixtures can be

481 understood by considering three main groups of TAG components: triunsaturated TAGs

482 (OOO and OOL), saturated-unsaturated-unsaturated TAGs (POO, POL, SOO) and

483 saturated-saturated-unsaturated TAGs (PPO). As confirmed by our previous work

484 (Bayés-García, Calvet, Cuevas-Diarte, Ueno, and Sato, ~~et al.~~ 2011, 2013a, 2013b,

485 Bayés-García, Calvet, Cuevas-Diarte, and Ueno, 2016b), TAGs belonging to the same

486 structural group display a highly similar polymorphic behavior.

487 Finally, by comparing the results obtained after analyzing the mixture of 6 TAG

488 components and EVOO, one may realize that, despite of some differences, the general

25

489 response, determined by DSC and XRD experiments, became considerably similar.

490 Thus we may conclude that the 6 main TAGs present in olive oil, which are OOO,

491 POO, OOL, POL, PPO and SOO, and approximately configure the 92% of its

492 composition, mostly determine their main polymorphic behavior. As to minor

493 components, they may not exert a strong influence in this case.

494

495

496 **4. Conclusions**

497 The characterization of the polymorphic behavior of multicomponent TAG mixtures,

498 formed by 2 to 6 TAGs permitted to make an approach to the understanding of a

499 complex natural lipid system, such as olive oil. The polymorphic behavior observed in

500 multicomponent TAG mixtures was interpreted by considering three main groups of

501 TAG components having different saturated-unsaturated molecular structures. We

502 observed that the polymorphic behavior of extra virgin olive oil obtained from the

503 Arbequina olive variety was mainly influenced by its main TAGs, whereas apparently

504 minor components did not develop a crucial role.

505 This may become a first step for defining the polymorphic behavior of olive oil to be

506 applied, for instance, for product authentication, the determination of food frauds or the

507 fractionation of this vegetable oil.

508

26

514 (proposals 2013G650, 2014G120, 2014G662). The authors also acknowledge the

515 Generalitat de Catalunya through the Grup Reconegut 2014SGR1208.

516

517 **References**

518

519 Akita, A., Kawaguchi, T., & Kaneko, F. (2006). Structural Study on Polymorphism of

520 Cis-Unsaturated Triacylglycerol: Triolein. *The Journal of Physical Chemistry B,* 110,

521 4346-4353.

522

523 Barba, L., Arrighetti, G., & Calligaris, S. (2013). Crystallization and melting properties

524 of extra virgin olive oil studied by synchrotron XRD and DSC. *European Journal of*

525 *Lipid Science and Technology,* 115, 322-329.

526

527 Bayés-García, L., Calvet, T., Cuevas-Diarte, M. A., Ueno, S., & Sato, K. (2011). *In situ*

528 synchrotron radiation X-ray Diffraction study of crystallization kinetics of polymorphs

529 of 1,3-dioleoyl-2-plamitoyl glicerol (OPO). *CrystEngComm,* 13, 3592-3599.

530

531 Bayés-García, L., Calvet, T., Cuevas-Diarte, M. A., Ueno, S., & Sato, K. (2013a). *In*

532 *situ* observation of transformation pathways of polymorphic forms of 1,3-dipalmitoyl-2-

533 oleoyl glycerol (POP) examined with synchrotron radiation X-ray diffraction and DSC.

534 *CrystEngComm,* 15, 302-314.

535

536 Bayés-García, L., Calvet, T., Cuevas-Diarte, M. A., Ueno, S., & Sato, K. (2013b).

537 Crystallization and Transformation of Polymorphic Forms of Trioleoyl Glycerol and

27

1,2-Dioleoyl-3-*rac*-linoleoyl Glycerol. *The Journal of Physical Chemistry BJ. Phys. Chem. B*, 117, 9170-9181.

Bayés-García, L., Calvet, T., Cuevas-Diarte, M. A., Ueno, S., & Sato, K. (2015). Phase Behavior of Binary Mixture Systems of Saturated-Unsaturated Mixed-Acid Triacylglycerols: Effects of Glycerol Structures and Chain-Chain Interactions. *The Journal of Physical Chemistry BJ. Phys. Chem. B*, 119, 4417-4427.

Bayés-García, L., Tres, A., Vichi, S., Calvet, T., Cuevas-Diarte, M. A., Codony, R., Boatella, J., Caixach, J., Ueno, S., & Guardiola, F. (2016a). Authentication of Iberian dry-cured ham: New approaches by polymorphic fingerprint and ultrahigh resolution mass spectrometry. *Food Control*, 60, 370-377.

Bayés-García, L., Calvet, T., Cuevas-Diarte, M. A., & Ueno, S. (2016b). In situ crystallization and transformation kinetics of polymorphic forms of saturated-unsaturated-unsaturated triacylglycerols: 1-palmitoyl-2,3-dioleoyl glycerol, 1-stearoyl-2,3-dioleoyl glycerol, and 1-palmitoyl-2-oleoyl-3-linoleoyl glycerol. *Food Research InternationalFood Res. Int.*, 85, 244-258.

Boodhoo, M. V., Bouzidi, L., & Narine, S. S. (2009). The binary phase behavior of 1,3-dipalmitoyl-2-stearoyl-*sn*-glycerol and 1,2-dipalmitoyl-3-stearoyl-*sn*-glycerol. *Chemistry and Physics of LipidsChem. Phys. Lipids*, 160, 11-32.

561 Bouzidi, L., Boodhoo, M. V., Kutek, T., Filip, V., & Narine, S. S. (2010). The binary

562 phase behavior of 1,3-dilauroyl-2-stearoyl-*sn*-glycerol and 1,2-dilauroyl-3-stearoyl-*sn*-

563 glycerol. *Chemistry and Physics of LipidsChem. Phys. Lipids*, 163, 607-629.

564

565 Chiavaro, E., Vittadini, E., Rodriguez-Estrada, M. T., Cerretani, L., & Bendini, A.

566 (2008). Differential scanning calorimeter application to the detection of refined hazelnut

567 oil in extra virgin olive oil. *Food Chemistry.*, 110, 248-256.

568

569 Chiavaro, E., Vittadini, E., Rodriguez-Estrada, M. T., Cerretani, L., Capelli, L., &

570 Bendini, A. (2009). Differential scanning calorimetry detection of high oleic sunflower

571 oil as an adulterant in extra-virgin olive oil. *Journal. of Food Lipids,* 16, 227-244.

572

573 Ferrari, C., Angiuli, M., Tombari, E., Righetti, M. C., Matteoli, E., & Salvetti, G.

574 (2007). Promoting calorimetry for olive oil authentication. *Thermochim.ica Acta.*, 459,

575 58-63.

576

577 Harwood, J. L., & Yaqoob, P. (2002). Nutritional and health aspects of olive oil.

578 *European Journal of Lipid Science and TechnologyEur. J. Lipid Sci. Technol.,*104, 685-

579 697.

580

581 Jiménez Márquez, A., & Beltrán Maza, G. (2003). Aplicación de la Calorimetría

582 Diferencial de Barrido (CDB) en la caracterización del aceite de oliva virgen. *Grasas y*

583 *Aceites*, 54, 403-409.

584

585   Jiménez Márquez, A., Beltrán Maza, G., Aguilera Herrera, M. P., & Uceda Ojeda, M.

586   (2007). Calorimetría diferencial de barrido. Influencia de la composición del aceite de

587   oliva virgen en su perfil térmico. *Grasas y Aceites*, 58, 122-129.

588

589   Ikeda, E., Ueno, S., Miyamoto, R., & Sato, K. (2010). Phase Behavior of a Binary

590   Mixture of 1,3-dipalmitoyl-2-oleoyl-sn-glycerol and 1,3-dioleoyl- 2-palmitoyl-sn-

591   glycerol in n dodecane Solution. *The Journal of Physical Chemistry B*~~J. Phys. Chem. B~~,

592   114, 10961 − 10969.

593

594   Larsson, K., Quinn, P., Sato, K., & Tiberg, F. (Eds.). (2006). *Lipids: Structure, physical*

595   *properties and functionality.* Bridgewater: The Oily Press.

596

597   Marangoni, A. G., & Narine, S. S. (Eds.). (2002). *Physical Properties of Lipids.* New

598   York: Marcel Dekker.

599

600   Mizobe, H., Tanaka, T., Hatakeyama, N., Nagai, T., Ichioka, K., Hondoh, H., Ueno, S.,

601   & Sato, K. (2013). Structures and Binary Mixing Characteristics of Enantiomers of 1-

602   Oleoyl-2,3-dipalmitoyl-*sn*-glycerol (S-OPP) and 1,2-Dipalmitoyl-3-oleoyl-*sn*-glycerol

603   (R-PPO). *Journal of the American Oil Chemists' Society*~~J. Am. Oil Chem. Soc.~~, 90,

604   1809-1817.

605

606   Salas, J. J., Bootello, M. A., Martínez-Force, E., & Garcés, R. (2011). Production of

607   stearate-rich butters by solvent fractionation of high stearic-high oleic sunflower oil.

608   *Food Chemistry*, 124, 450-458.

609

610 Sasaki, M., Ueno, S., & Sato, K. (2012). Polymorphism and Mixing Phase Behavior of

611 Major Triacylglycerols of Cocoa Butter. In N. Garti, & N. R. Widlak (Eds.), *Cocoa*

612 *Butter and Related Compounds* (pp. 151-172). Urbana: AOCS Press.

613

614 Timms, R. E. (2005). Fractional crystallization – the fat modification process for the

615 21st century. *European Journal of Lipid Science and Technology*~~Eur. J. Lipid Sci.~~

616 ~~Technol.~~, 107, 48-57.

617

618 van Mechelen, J. B., Peschar, R., & Schenk, H. (2008). Structures of mono-unsaturated

619 triacylglycerols. IV. The highest melting β'-2 polymorphs of *trans*-mono-unsaturated

620 triacylglycerols and related saturated TAGs and their polymorphic stability. *Acta*

621 *Crystallographica*~~Cryst.~~, B64, 249-259.

622

623 Yano, J., Kaneko, F., Kobayashi, M., Kodali, D., Small, D. M., & Sato, K. (1997).

624 Structural Analyses and Triacylglycerol Polymorphs with FT-IR Techniques. 2. β'1-

625 Form of 1,2-Dipalmitoyl-3-myristoyl-*sn*-glycerol. *The Journal of Physical Chemistry*

626 *B*~~J. Phys. Chem. B~~, 101, 8120-8128.

627